Pergamon

PII: S0191–8141(98)00012–1

Journal of Structural Geology, Vol. 20, No. 7, pp. 827 to 840, 1998

0191-8141/98 $19.00 + 0.00

Reliability of palaeostress analysis from fault striations in near multidirectional extension stress fields. Example from the Ebro Basin, Spain

L. E. ARLEGUI-CRESPO and J. L. SIMON-GOMEZ

Departamento de Geología, Plaza San Francisco Universidad de Zaragoza, Spain (arlegui@posta.unizar.es)

(*Received* 13 *August* 1997; *accepted in revised form* 29 *January* 1998)

Abstract—A standard palaeostress analysis was carried out by applying a sequence of the Right Dihedra, y–R diagram and Etchecopar methods to 37 fault samples collected in Miocene deposits of the central Ebro Basin. This gave rise to 37 *standard solutions* which show a pervasive multidirectional extension stress regime for this region. Owing to the possible low definition of the horizontal stress axes in this type of stress regime, the results were then submitted to a stability test by subsampling the initial data sets. The level of stability of the solutions is good, as defined by the differences between successive solutions and the standard one. Most individual stress tensors so obtained differ by less than 15° in σ_3 azimuth and 0.1 in stress ratio $R = (\sigma_2 - \sigma_3)/(\sigma_1 - \sigma_3)$, respectively, from the corresponding standard solutions. Furthermore, the application of the Central Limit Theorem by averaging solutions from groups of subsamples demonstrates that the majority of the *standard* stress tensors are quite exact. The regional homogeneity of the final results is interpreted as a further proof of reliability.

Stability and reliability increase as the sample size grows. There is no 'magic' number of data which separates reliable from unreliable stress solutions, but a quantitative approach allows us to estimate the expected error and the associated probability for each sample size. A sufficient stability may be accomplished using monophase fault samples from 25–30 faults, and it does not increase significantly for samples larger than 40 faults. For samples under 20–25 faults in uniaxial stress regimes (especially in multidirectional extension), the subsampling/averaging technique may be a useful tool. This method also allows testing and, in some special cases (these where subsample mean tensors provide stable results that systematically differ from the initial standard tensor), improving stress solutions.

INTRODUCTION

The type of stress regime where the σ_1 axis is vertical and σ_2 approaches σ_3 is usually designed as radial or multidirectional extension (Armijo, 1977). Obviously, the stress ellipsoid need not to be exactly uniaxial, so σ_2 and σ_3 may be slightly different. In the case of $\sigma_2 = \sigma_3$ the stress state will be referred as pure multidirectional extension. This type of tectonic stress is common in intraplate zones which have undergone slight to moderate extensional tectonics, frequently accompanied by vertical uplift: Arabian Platform (Hancock *et al.*, 1987), Iberian Chain, Jaca Basin and Ebro Basin, within the Iberian Peninsula (Simón-Gómez, 1989; Turner and Hancock, 1989; Arlegui and Simón, 1993), South Wales (Dunne and North, 1990; Caputo, 1995).

Orthogonal, *grid-lock* joint patterns (Hancock *et al.*, 1987) perhaps constitute the most pervasive structural style in this tectonic environment (Fig. 1a). Although they have sometimes been attributed to successive fracturing episodes under changing external forces (Park, 1983; Hancock, 1985), recent works have demonstrated that they can be a consequence of internal, small-scale stress redistribution within stable multidirectional extension stress fields. Briefly, when a primary set of tensional fractures develops normal to σ_3, the release of tension causes swapping of the σ_2 and σ_3 axes and, eventually, the formation of new fractures abutting the former ones at right angles (Simón *et al.*, 1988; Simón-Gómez, 1989; Caputo, 1995). The presence of such orthogonal joint systems allows a very accurate interpretation of the σ_2 and σ_3 trends, although no quantitative approach to the stress ratio can be made.

Quite different is the case of faults. In some cases, multidirectional extension gives rise to systematic conjugate normal faults, following either one or two orthogonal strikes (Fig. 2a & b). However, very often they show a high variability of directions; in some extreme cases they make up 'complete strike fans' (Fig. 2c) or develop conical fault surfaces (Fig. 1b). The reconstruction of palaeostresses from striated fault populations is an important tool for tectonic interpretation, which has been broadly performed in a variety of structural settings. However, it has some difficulty in providing reliable results in near uniaxial extension regimes. For instance, if we use any current method, based on Bott's equation (Bott, 1959), we normally obtain a precise value of the stress ratio, but the directions of the horizontal stress axes may not be well defined owing to the similarity between σ_2 and σ_3. Some scepticism about the reliability of the inferred orientations may then arise, so that a further test beyond the standard analysis is necessary.

In this paper we show the results of applying systematically a test of reliability to palaeostresses

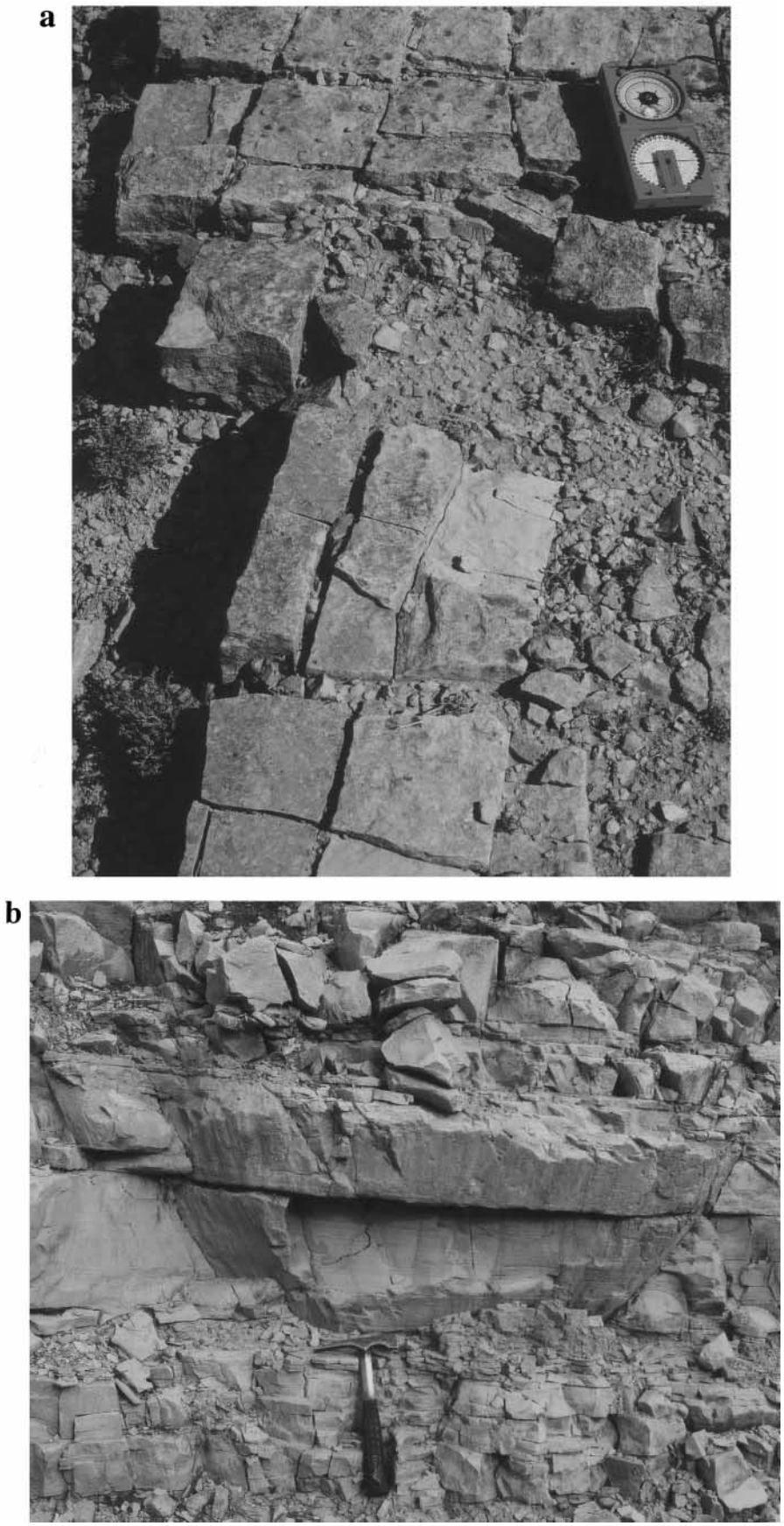

Fig. 1. Different fracture styles in multidirectional extension stress fields; examples from the central Ebro Basin, Spain (see location of outcrops in map of Fig. 3). (a) Orthogonal joint system (station Zar-2). (b) Conical fault surface (station Rem-2).

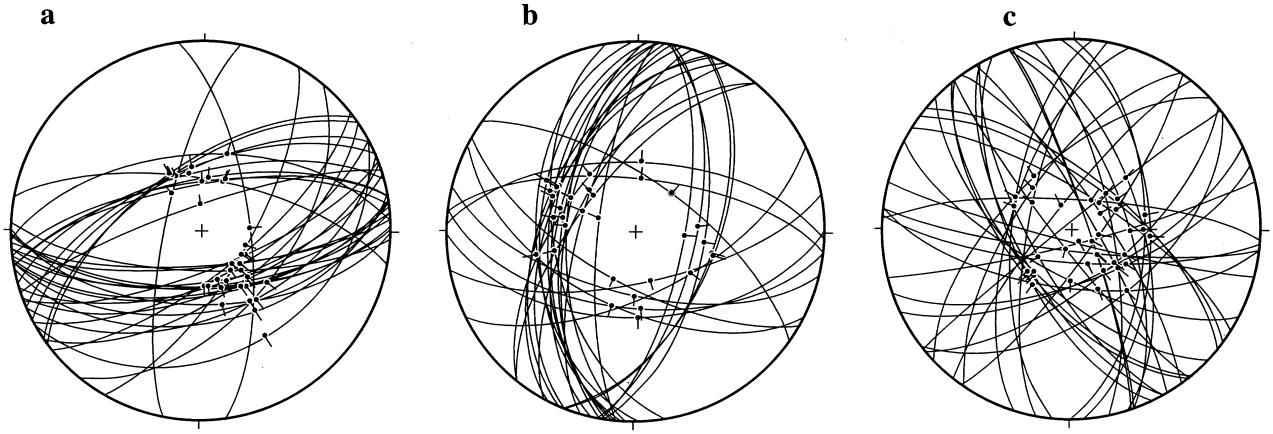

Fig. 2. (a) Conjugate normal faults in station Meq-13 (equal-area plot of planes and striations, lower hemisphere). (b) Two orthogonal systems of conjugate normal faults (station Rem-2). (c) Normal faults showing a 'complete strike fan' (station Lon-8).

obtained from a number of fault samples measured in Neogene deposits of the central Ebro Basin. The calculated stress ratio $R = (\sigma_2 - \sigma_3)/(\sigma_1 - \sigma_3)$ is close to 0 in most cases, and indicates that the regional stress field corresponds to a multidirectional extension regime. First we will analyse the stability of stress tensors by means of a 'subsampling' technique similar to that used by Reches *et al.* (1992). Afterwards, we will demonstrate that the stable solutions so obtained are reliable, that is to say they are representative of the total fault population and they express the actual stress field. At the same time we are discussing an important methodological question in palaeostress analysis: the minimum number of data necessary for an accurate definition of the local stress tensor.

GEOLOGICAL SETTING

The Tertiary Ebro Basin, located in the northeastern Iberian Peninsula, is framed by three mountain ranges, the Pyrenees, the Iberian Chain and the Catalonian Coastal Ranges (see Fig. 3). The tectonic development of those chains controlled the structural and sedimentary basin evolution. Nevertheless, the Ebro Basin evolved mainly as the southern foreland basin of the

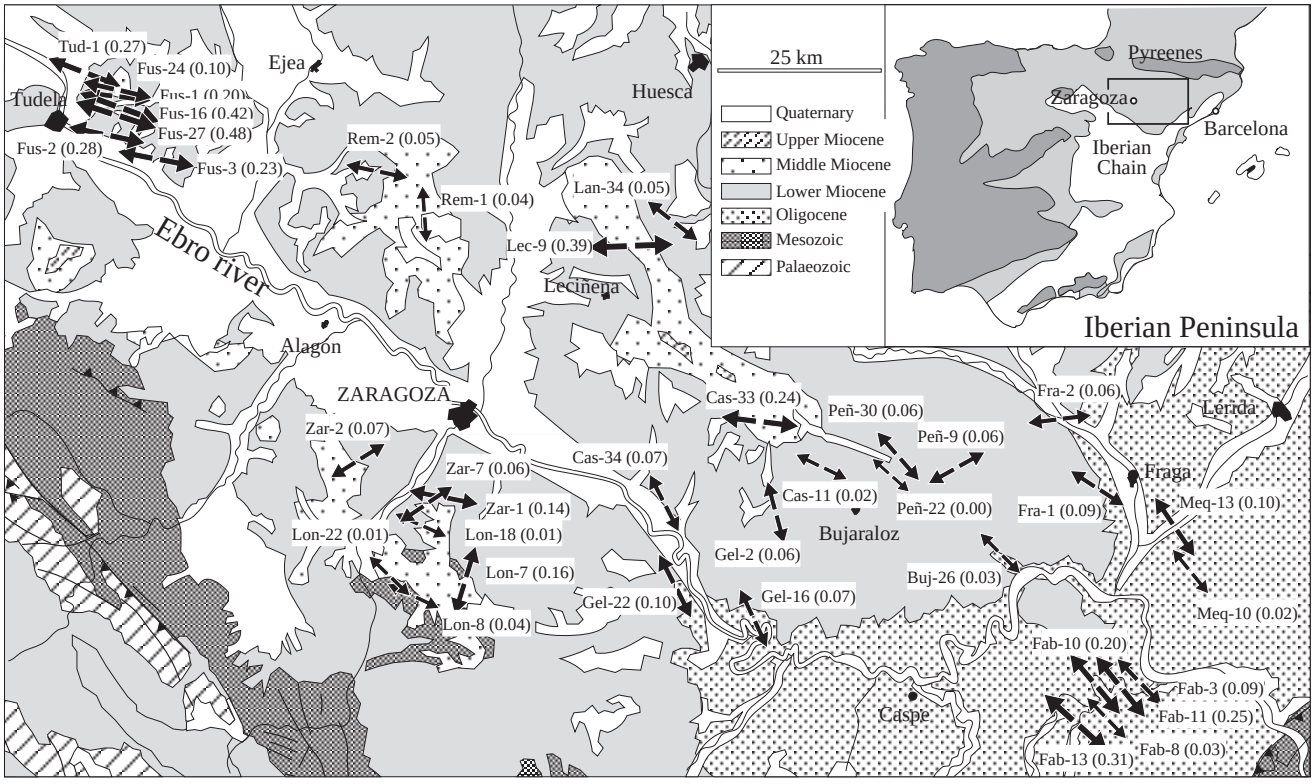

Fig. 3. Map of extensional palaeostresses in the central Ebro Basin. Arrows indicate the directions of σ_3 obtained as final solutions in the analysed stations; arrow size relates to R value. Stress ratio $R = (\sigma_2 - \sigma_3)/(\sigma_1 - \sigma_3)$.

Table 1. Characteristics of the measure stations, fault samples and stress tensors inferred from them. See location of sites on the map of Fig. 3. The *standard solutions* are obtained by applying the combination of Right Dihedra, y–R and Etchecopar methods (see explanation in text). The *final solutions* arising from the *subsampling/averaging technique* are listed only for stations in which they differ from the standard solutions. Their σ_1 axes are near vertical in every case, so that only orientation of σ_3 and stress ratio $R_e = (\sigma_2 - \sigma_3)/(\sigma_1 - \sigma_3)$ are given

				Standard solution		Final solution	
Station	UTM	Bedding	No. of faults	σ_3	R_e	σ_3	R_e
Buj-26	31TBF582904	Horizontal	29	135, 00	0.03	?	
Cas-11	30TYM323045	Horizontal	23	116, 00	0.02		
Cas-33	30TYM228117	Horizontal	8	097, 05 E	0.24		?
Cas-34	30TYM81991	Horizontal	28	153, 01 S	0.07	150, 01 N	0.09
Fab-3	31TBF761685	Horizontal	29	136, 02 S	0.04	144, 01 S	0.09
Fab-08	31TBF	Horizontal	25	136, 07 W	0.03		
Fab-10	31TBF711692	Horizontal	24	140, 00	0.20		
Fab-11	31TBF734679	Horizontal	48	141, 02 W	0.25		
Fab-13	31TBF685643	Horizontal	8	132, 08 S	0.31		?
Fra-1	31TBF730994	Horizontal	22	123, 04 E	0.09	?	?
Fra-2	31TBG688105	Horizontal	8	083, 06 E	0.06		
Fus-1	30TXM245616	Horizontal	52	101, 02 E	0.22		?
Fus-2	30TXM307507	046 11 N	15	102, 10 W	0.28		
Fus-3	30TXM313498	058 08 S	21	097, 05 E	0.23		0.20
Fus-16	30TXM245612	074 06 N	47	110, 02 E	0.42		0.27
Fus-24	30TXM242615	Horizontal	14	103, 00	0.10		
Fus-27	30TXM246608	Horizontal	56	108, 06 W	0.48		
Ge-2	30TYL252974	Horizontal	20	149, 02 W	0.02	162, 01 E	0.06
Ge-16	30TYL218813	Horizontal	15	146, 10 E	0.07	153, 10 E	
Ge-22	30TYL106864	Horizontal	20	136, 03 E	0.02	154, 05 W	0.10
Lan-34	30TYM063340	Horizontal	10	128, 11 E	0.05		
Lec-9	30TYM054330	Horizontal	25	087, 02 E	0.45		0.39
Lon-7	30TXL755862	Horizontal	16	017, 01 N	0.16		
Lon-8	30TXL690872	Horizontal	38	115, 02 E	0.01	?	0.04
Lon-18	30TXL687947	Horizontal	54	124, 02 E	0.01		
Lon-22	30TXL640882	Horizontal	70	132, 00	0.01		
Meq-10	31TBF877857	Horizontal	19	141, 01 W	0.02		
Meq-13	31TBF837919	Horizontal	36	146, 00	0.10		
Peñ-9	31TBG523044	Horizontal	18	061, 00	0.04		0.06
Peñ-22	30TYM437040	Horizontal	12	132, 11 W	0.00	?	
Peñ-30	30TYM435052	Horizontal	13	139, 02 W	0.06		
Rem-1	30TXM718432	085 11 S	30	006, 01 S	0.02		0.04
Rem-2	30TXM693483	Horizontal	34	102, 00	0.05		
Tud-1	30TXM175624	Horizontal	35	111, 00	0.27		
Zar-1	30TXM738001	Horizontal	14	101, 00	0.14		
Zar-2	30TXM595065	Horizontal	54	068, 00	0.05	0.58, 01 W	0.07
Zar-7	30TXM704002	Horizontal	22	055, 09 W	0.06		

Pyrenees, and most of its structural features are related to this tectonic situation. The basin is nearly asymmetric, with its deepest trough under the Pyrenees (the depth of the pre-Tertiary substratum increases northwards, reaching values of 4000 m under the sea level below the Pyrenees; Riba *et al.*, 1983). The Ebro Basin is also an intraplate region within the Iberian plate, and was affected by the tectonic evolution of the northeastern Iberian peninsula during the Neogene age (Simón-Gómez, 1989).

The studied area is located in the central part of the Ebro Basin. Most rocks are of Oligocene–Miocene age (including clastic, evaporite and carbonate facies) of a fluvial and lacustrine origin (Riba *et al.*, 1983). The beds are almost flat-lying except where there are local buoyant rise of evaporites or map-scale normal faults with associated roll-over anticlines. The main macrostructural feature in the area is the Logroño–Sástago syncline (Quirantes, 1978; Arlegui *et al.*, 1997), a wide NW–SE-trending fold of gentle dipping (up to 4–6°) located along the Ebro River.

STANDARD RESULTS OF PALAEOSTRESS ANALYSIS FROM FAULT POPULATIONS

Palaeostress analysis has been performed from fault populations collected in 37 outcrops in the central Ebro Basin. The faults affect Miocene limestones and marls showing horizontal or gently dipping bedding (see Table 1). A total of 1012 decimetric- to metric-scale fault planes and striations have been measured and analysed. Most of them are normal faults dipping from 55 to 75° and showing striation pitches from 75 to 90°. Only a very few strike-slip faults were observed. The sense of movement has been determined in the majority of faults by observing kinematical indicators, usually Riedel fractures (secondary synthetic fractures and lunate fractures, both types appertaining to the group R of Petit, 1987).

The analysis of data has been made by using a sequence of three methods, each one providing a different approach to the stress determination problem, whose joint usefulness has been broadly tested in the

past years (Casas *et al.*, 1990, 1992; Casas and Maestro, 1996; Arlegui, 1996) and enables the complete definition of stress tensors:

(a) *Right Dihedra method* (Pegoraro, 1972; Angelier and Mechler, 1977). This is a simple geometrical approach which provides an initial estimate of stress directions.
(b) *y–R diagram* (Simón-Gómez, 1986). It is a 2D approximation in which one of the principal stress axes is supposed to be vertical, so that tensors may be represented only by two parameters: y (azimuth of the maximum horizontal stress, σ_y) and R (stress ratio in Bott's equation, $R = (\sigma_z - \sigma_x)/(\sigma_y - \sigma_x)$). The y, R pairs satisfying one individual fault give rise to a curve; the 'knots' where these curves intersect show a preliminary spectrum of all possible solutions and their relative weight in the whole fault population (especially useful in the case of polyphase tectonics).
(c) *Etchecopar's method* (Etchecopar *et al.*, 1981; Etchecopar, 1984). This is a numerical method which allows the exploration of the solutions suggested by the *y–R* and Right Dihedra diagrams. These solutions will eventually be confirmed and refined in order to obtain the final, complete solution: 3D orientations of the three principal stress axes and stress ratio. Among the variety of numerical methods sharing a similar approach, Etchecopar's is a particularly strong method. Based upon the minimization of the angles between real and theoretical striations, it allows the separation of different stress tensors by means of an adequate management of the percentage of data submitted to minimization. In monophase populations a satisfactory solution is normally obtained for 80–90% of faults, thus rejecting 10–20% of spurious data. In suspected polyphase populations the initial required percentage should be lower (30–50%); the program chooses the best fitting faults representing this initial percentage, which are then discarded in order to find a second stress solution.

In our case, the first two methods usually provide ambiguous results owing to the radial or multidirectional character of the extensional stress. An example is shown in Fig. 4 (station Rem-2, see location in Fig. 3). In the Right Dihedra diagram (Fig. 4a) almost every horizontal direction is compatible with an extensional axis for 90% of faults. In the *y–R* diagram (Fig. 4b) the curve intersections do not show any clear 'knot' but a long band with two near orthogonal maxima; the high R ratio is well established (indicator of radial extension) whereas the azimuths of σ_2 and σ_3 are not defined. Unfortunately, this graphical ambiguity does not disappear if a similar method such as proposed by Fry (1992) is utilized. Grid methods, as those proposed by Etchecopar (1984, Monte Carlo method), Galindo and González (1988) and Gephart (1990), provide a similar exploration of possible solutions. They would be of interest in the case of polyphase populations; nevertheless, in a single phase population like ours, the Right Dihedra and *y–R* diagrams perform this initial exploration as well. The method of Etchecopar *et al.* (1981) always gives an accurate calculation of the optimum σ_3 direction and R ratio. For instance, in station Rem-2, a stress tensor similar to that represented by the left knot in the *y–R* diagram has been chosen as the best solution (Fig. 4c). However, the errors estimated by the computer program are sometimes too high (in this case, error of σ_3 azimuth = 59°) and the result may not necessarily be reliable.

The stress tensors obtained after standard analysis using these methods have been compiled in the corresponding columns of Table 1. Details of situation, bedding and number of faults in each outcrop are also given. All these stress tensors have been taken as *standard solutions* which will be next submitted to the stability test.

STABILITY OF STRESS SOLUTIONS: THE *SUBSAMPLING* TEST

If an actual palaeostress state was responsible for the fault striations observed in an outcrop, the former should be able to be inferred from any representative sample of such striated faults. That is to say the analysis of any random combination of a sufficient number of data should give stable results.

In order to check for such stability, and with inspiration from statistical bootstrapping techniques, each fault population explained by a *standard solution* has been submitted to subsampling by discarding a number of data at random. The number of discarded data is progressively increased, so that subsamples become smaller and approach the absolute minimum number (four faults) needed for obtaining an algebraic solution. As an example, in station designated as Fab-11, the following subsampling sequence has been carried out starting from an initial sample of 48 faults: four subsamples of 40–45 faults, seven subsamples of 33–38 faults, 10 subsamples of 25–30 faults, 11 subsamples of 16–20 faults, 11 subsamples of 10–15 faults and 13 subsamples of six–nine faults. It is not advisable to take subsamples very close to the initial number, since they are expected to show a behaviour which resembles too closely the original sample. Neither is it advisable to take subsamples under six faults.

Following the former criteria each station gives rise to a number of subsamples (normally between 20 and 60 in number) which are separately submitted to analysis by the Etchecopar method. Almost every fault sample represents a monophase population, that is to say it may be adequately explained by a single stress tensor. Nevertheless, the standard tensor need not be compatible with exactly 100% of the extensional faults. So the percentage introduced for running

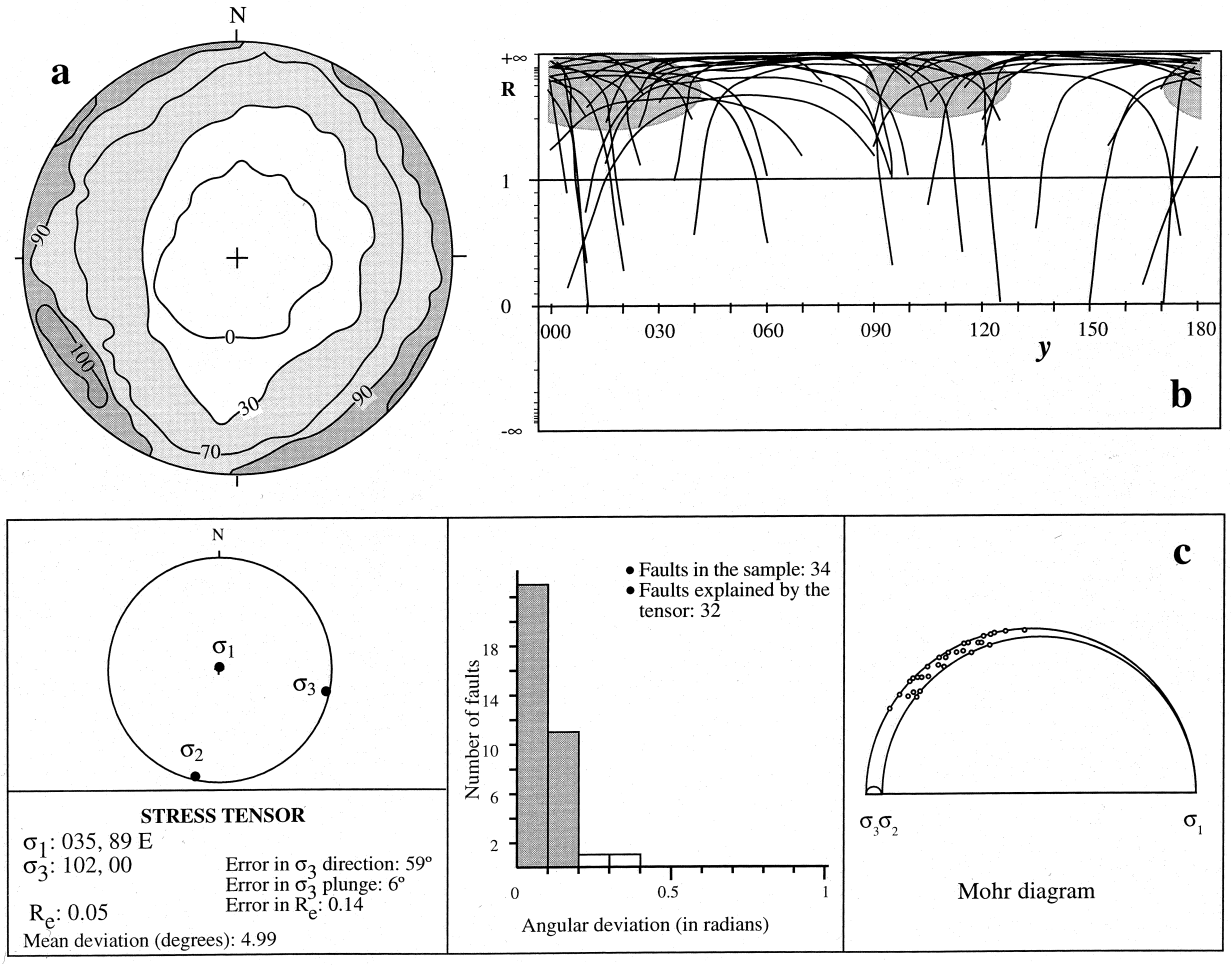

Fig. 4. Example of standard stress analysis of a fault population (station Rem-2). See location on map of Fig. 3 and equal-area plot of fault data in Fig. 2(c). (a) Right Dihedra diagram (Schmidt net, lower hemisphere); isolines express the percentage of faults compatible with an extension axis. (b) y–R diagram; y is the azimuth of the maximum horizontal stress σ_y; $R = (\sigma_z - \sigma_x)/(\sigma_y - \sigma_x)$; the shaded ellipses indicate the zones showing the highest density of curve intersections, and so the optimum stress tensors. (c) Results of Etchecopar's method: stereoplot of the inferred stress axes, $R_e = (\sigma_2 - \sigma_3)/(\sigma_1 - \sigma_3)$; histogram of angular deviations between actual striation and theoretical shear component on each fault; Mohr diagram where the planes corresponding to the explained faults are plotted.

Etchecopar's program should be adjusted in each case in order to optimize the solution according to the usual criteria for this method. In our analysis this percentage ranged from 80 to 100%. Only in one case (station Fab-03) a second compressional stress state has been inferred; the faults corresponding to this second tensor have been discarded and the stability analysis has been applied to the main extensional tensor.

Figure 5 shows the results of applying the stability test to the station Fab-11 (see location in Fig. 3). Differences between the σ_3 azimuth obtained from each subsample ($S_{3\text{sam}}$) and that of the standard solution ($S_{3\text{std}}$) are plotted vs the subsample size (Fig. 5a). In the same way, differences in R values ($R_{\text{sam}} - R_{\text{std}}$) are also plotted (Fig. 5b). The absolute values of these differences are obviously larger for small subsamples (less stable solutions). Figure 5(c–f) shows the mean values and standard deviations of the two former parameters ($S_{3\text{sam}} - S_{3\text{sta}}$ and $R_{\text{sam}} - R_{\text{std}}$) calculated for every group of subsamples of the same size. Standard deviations clearly express how variability diminishes as subsample size increases; the deviations decrease significantly for subsamples over 15 faults and become practically zero for subsamples larger than 35 faults.

On the other hand, the mean values show another interesting (and perhaps surprising) result: for every sample size the mean difference ($S_{3\text{sam}} - S_{3\text{std}}$) is close to 0. In practice, as the obtained σ_3 axes are always very close to horizontal, this implies that the direction of the mean σ_3 vector practically equals that of the standard solution (azimuth of mean $\sigma_3 \approx S_{3\text{std}}$). Mean values of $R_{\text{sam}} - R_{\text{std}}$ are a little more variable, but they also approach 0. So the mean stress tensors obtained from groups of subsamples are very close to the standard tensor from the initial, relatively large sample.

The same test described above for the station Fab-11 was applied to each of the 37 stations studied in the region. The results show significant differences in the stability of their solutions. Many stations provide

stress results as good as those of Fab-11, whereas others show instabilities either in orientation (σ_3 azimuth) or stress ratio. Three examples are compiled in Fig. 6. Instabilities in σ_3 azimuth are easier to be found, logically, in cases of fault populations showing 'complete strike fans', such as station Lon-8 (see equal-area plot of fault data in Fig. 2c). For this case, the R ratio has been calculated with an accept-

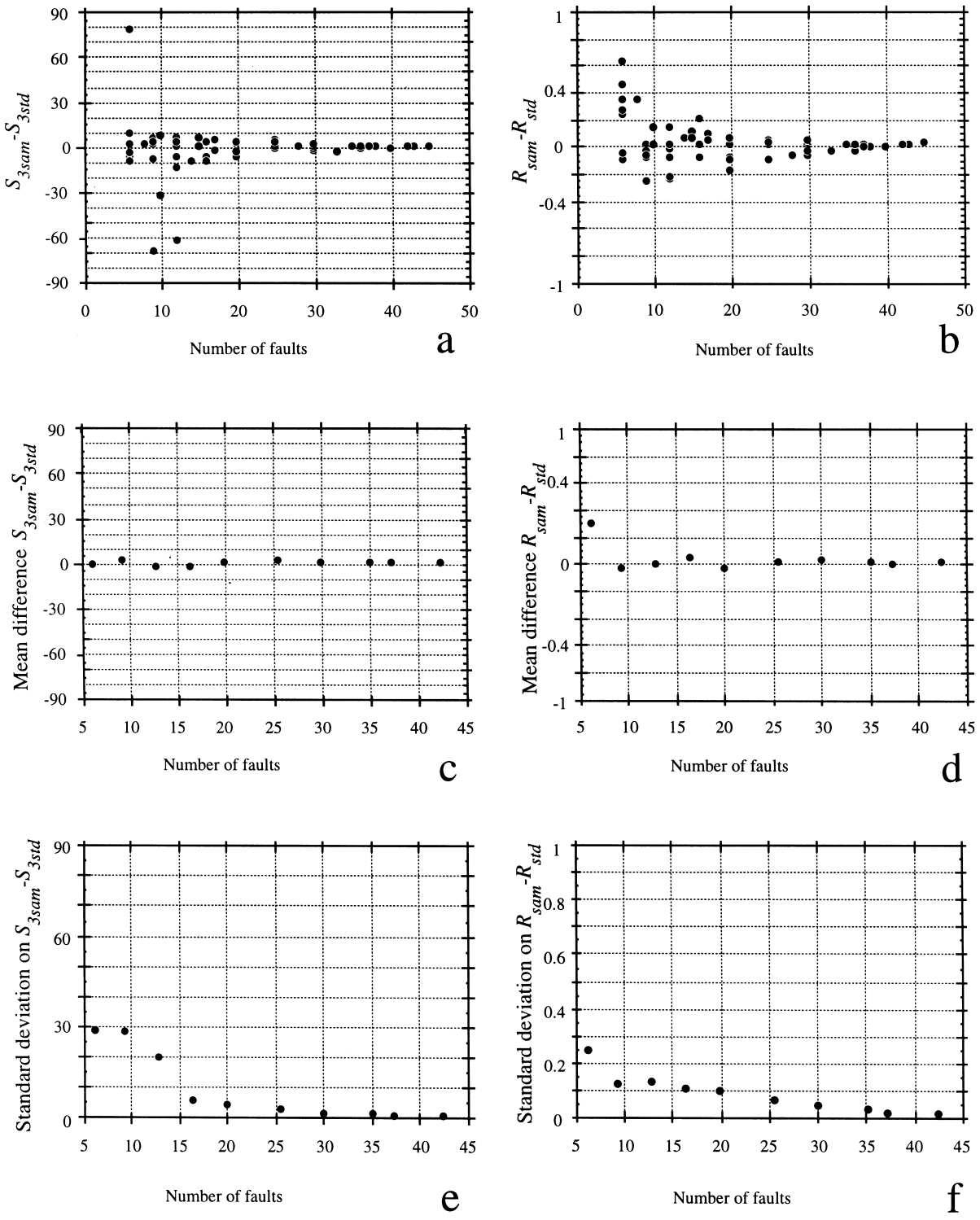

Fig. 5. Results of applying the stability test to the station Fab-11 (see location in Fig. 3). Number of faults of the initial sample: 48. Number of subsamples analysed: 56. $S_{3\mathrm{sam}}$: azimuth of σ_3 obtained for each subsample. $S_{3\mathrm{std}}$: azimuth of σ_3 corresponding to the *standard solution*. R_{sam}: stress ratio $(\sigma_2-\sigma_3)/(\sigma_1-\sigma_3)$ of tensors obtained for each subsample. R_{std}: stress ratio of the *standard solution*. Abscise: number of faults of subsamples. (a) and (b) Individual results for each subsample. (c) and (d) Mean values for groups of subsamples of the same size. (e) and (f) Standard deviations for groups of subsamples.

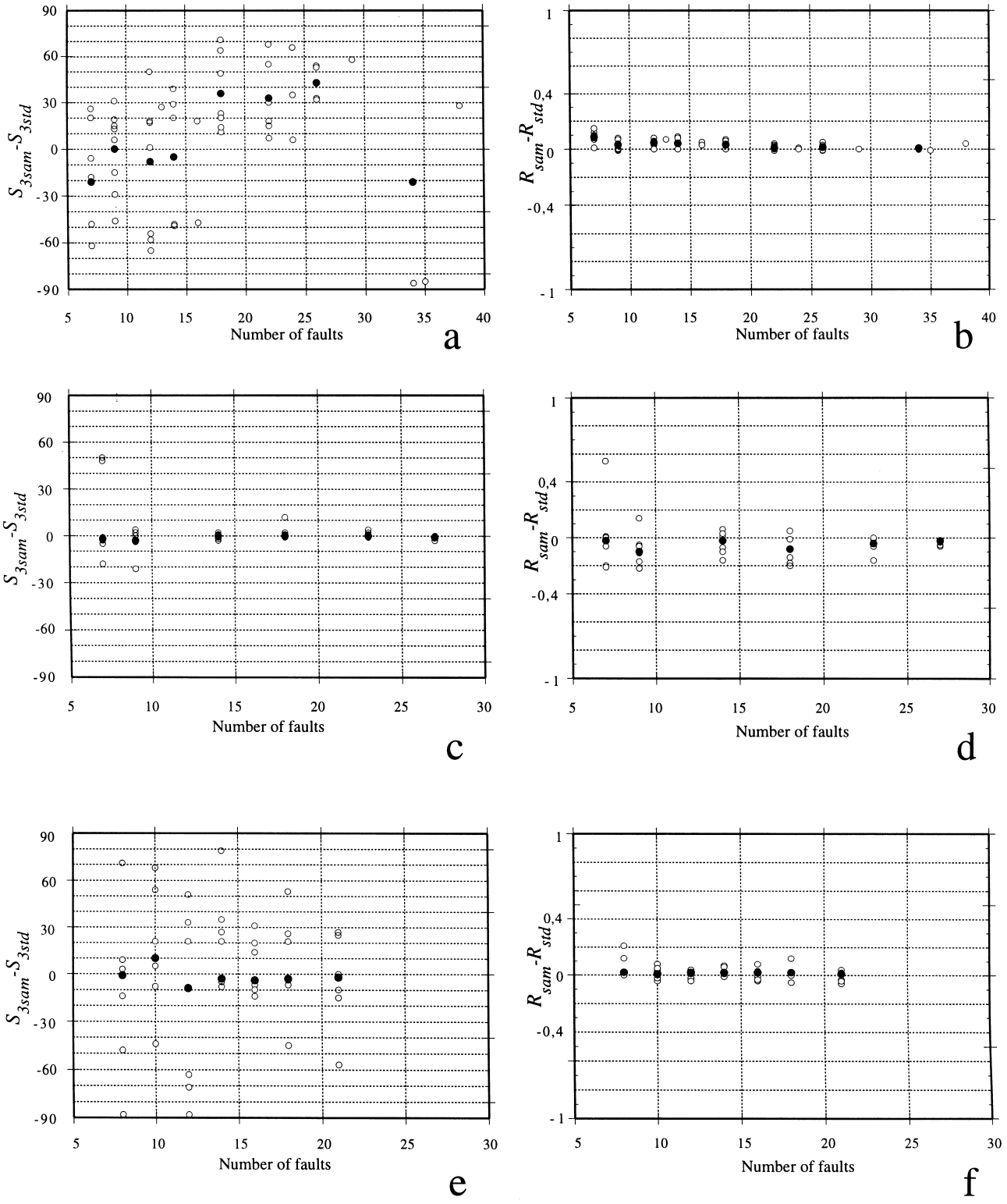

Fig. 6. Summarized results of stability tests applied to stations Lon-8 (a & b), Fus-3 (c & d) and Cas-34 (e & f). The differences ($S_{3sam}-S_{3std}$) and ($R_{sam}-R_{std}$) are plotted for each subsample (open circles) together with the corresponding means for groups of subsamples of the same size (black circles).

able precision (Fig. 6b), whereas the orientation of σ_3 is completely unstable for samples of every size (Fig. 6a). Instabilities in R ratio are mainly found in near conjugate fault systems such as found in station Fus-3; the corresponding fault sample provides a good determination of the stress axes (Fig. 6c) but gives less precise values of stress ratio (Fig. 6d). We should remember that, according to Bott's equation, the direction of movement on any fault plane parallel to one of the principal stress axes does not depend upon the R

ratio (Bott, 1959). Station Cas-34 represents an intermediate, quite usual level of stability (Fig. 6e & f).

Nevertheless, the whole results of stability tests applied to the 37 studied stations suggest that the stress solutions listed in Table 1 are in general quite stable. These results are summarized in Fig. 7 using the same format as Fig. 5. The tendencies pointed out in the station Fab-11 are now confirmed and region-

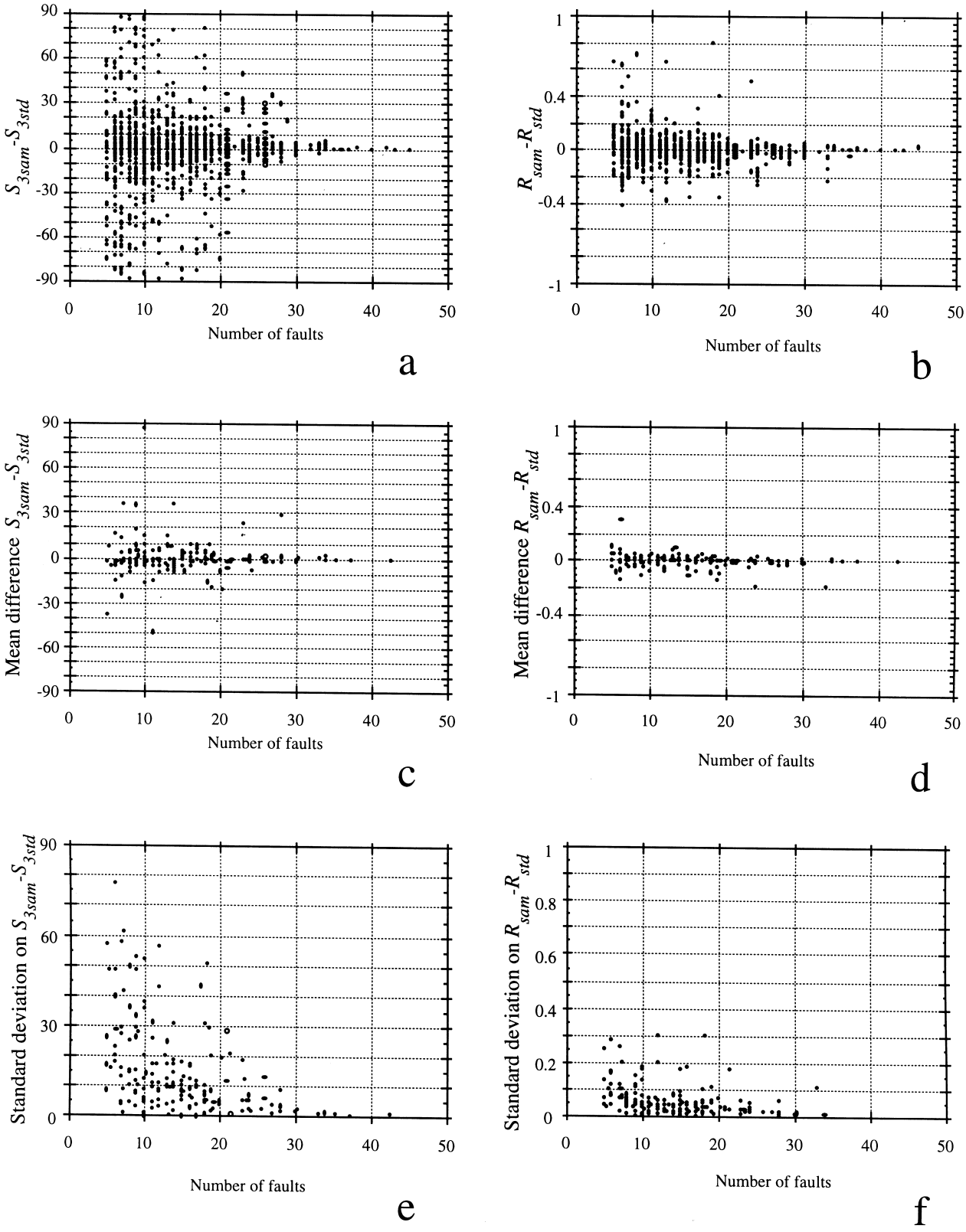

Fig. 7. Synthetic results of the stability test for the whole of stations studied in the region. Number of stations/samples: 37. Number of subsamples analysed: 1781. The plotted variables are the same as those of Fig. 5.

ally extended. Both ($S_{3sam}-S_{3std}$) and ($R_{3sam}-R_{3std}$) differences tend to approach 0 as subsample size increases (Fig. 5a & b). This tendency is stronger for mean values obtained for groups of subsamples of the same size (Fig. 7c & d). Most of the mean σ_3 directions and mean R values differ less than 10° and 0.1, respectively, from the standard solution, even for quite small fault numbers. Finally, standard deviations plotted in Fig. 7(e & f) show that the dispersion of results increases for small subsamples, though most subsamples over 10 faults show standard deviations under 20°.

Some useful methodological consequences arise from the above analysis. We can consider that any of our artificial subsamples might be an actual sample directly measured in the outcrop. So the stability shown by these subsamples may be seen as the stability of equivalent actual samples of the same characteristics. The following conclusions can be stated:

(1) The precision or stability of palaeostress solutions from fault population analysis logically depends upon the sample size. So, as a general rule, data collection should be as intensive as possible.
(2) In multidirectional extension regime, the Etchecopar method provides very precise and stable palaeostress solutions using monophase fault samples from about 25–30 faults. Stability does not increase significantly for samples larger than 40 faults. No stability test is required in such cases.
(3) The stability of results diminishes for samples under 25 faults, although the dispersion extends symmetrically around the standard solution. This pattern seems to be present even for samples close to the minimum necessary for the algebraic determination of the stress tensor (four faults). This allows the application of the *subsampling/averaging technique*: dividing the initial sample into groups of subsamples progressively smaller; applying the Etchecopar method to those subsamples, and obtaining the mean result from each group. The similarity of these mean tensors to each other, as well as the dispersion pattern of the solutions obtained from the whole of subsamples, will express the level of stability of the result. Figures 5 and 6 enable us to compare examples of good quality, stable solutions and poor quality, unstable solutions, respectively. The first ones show a very small dispersion for large subsamples, and the instability systematically increases as subsample size diminishes (Fig. 5). Poor quality solutions are characterized by random patterns showing high dispersion virtually for every subsample size (Fig. 6a & d).

RELIABILITY OF STRESS SOLUTIONS: THE EXTENSIONAL STRESS FIELD IN THE EBRO BASIN

After seeing that our stress solutions are quite stable we also need to prove that they are reliable. From the statistical point of view, reliability implies that the result obtained from a sample is representative of the whole population. For our purpose, reliability means that the stress solutions are not an artefact, and that they really represent tectonic stress states which actually existed in the region. We will discuss this problem using both statistical and geological arguments, in order to obtain a believable model of the regional Neogene stress field in the Ebro Basin.

A *precise* measure or a *stable* result need not be exact. They may contain systematic errors caused by bias either in measuring or analysing. Evaluating exactitude implies the knowledge of the 'true' measure or result, which only can be rigorously accomplished by other independent approaches. In our case, the use of regional joint sets might constitute such an independent approach for reconstructing palaeostress directions. But, unfortunately, they are only partially syngenetic with respect to faults, and their interpretation involves many problems derived from the superposition of different stress fields (Arlegui, 1996).

A statistical approach to the meaning and reliability of our *stable* palaeostress results is feasible by applying the Central Limit Theorem. After this theorem, if we take a number of samples from a data population which is quite large with respect to the sample size, the sample means show a normal distribution around the mean of the population (Till, 1974). This will occur for virtually all types of distributions. In our case we are not dealing with simple means of values, but with mean stress tensors obtained from fault data after a complicated analytical procedure. Nevertheless, Stuart (1984) demonstrated that the Central Limit Theorem is also true in this case.

Reches *et al.* (1992) proposed a procedure of palaeostress analysis which is based upon this principle and allows stability checking of palaeostress results in a similar way to that used in this work. These authors improved the inversion method of Reches (1987) by means of an evaluation of the confidence limits, which is accomplished by sampling with replacement. In their calculations the original cluster of K faults is resampled with random selection of additional samples, each with K faults. This implies that the additional samples may contain some of the original data more than once. The mean parameters of the tensors obtained from these samples show a normal distribution around the mean stress tensor for the original population (Stuart, 1984).

According to this theory, the mean stress tensors represented in Figs 5(c & d), 6 and 7(c & d) for groups of subsamples (which may be seen as true, diverse samples corresponding to the same fault population) should be considered as the best approach to the actual palaeostress states. Of course it is always necessary to be sure that those mean tensors constitute a stable ensemble.

In most cases the application of these criteria enables to state that the standard solutions listed in Table 1 are quite reliable. This occurs when the basic parameters defining the mean tensors (σ_3 azimuth, R ratio) approach closely those of the standard solution for every subsample group (see Fig. 5c & d). In a number of cases, the parameters of those mean tensors are quite stable but diverge systematically from the standard tensor in a given quantity. For instance, subsamples from station Cas-34 show systematic differences $(S_{3sam}-S_{3std}) \approx -3^\circ$ and $(R_{3sam}-R_{3std}) \approx +0.02$ (Fig. 6e & f). Then the solution should be revised considering the new results provided by the subsampling/averaging technique. In the previous example, the standard stress parameters listed in Table 1 for station Cas-34 (σ_3: 153, 01 S; $R = 0.07$) were modified to σ_3: 150, 01 N; $R = 0.09$. Slight modifications of this type were made in 12 stations (see Table 1). Finally, in a few samples, the instability of the mean tensors does not allow us to decide if the standard solution is the 'exact' solution, but neither do we have any criterion for modifying the former. A question mark is then written in the corresponding column of Table 1.

Geological arguments for the reliability of palaeostress results come from the comparison of the stress tensors obtained all over the studied region, namely the central Ebro Basin. The final solutions adopted in each site after applying the subsampling/averaging technique (which differ very little from the standard solutions, as we have seen) are compiled in the map of Fig. 3. The homogeneity of most results (both the σ_3 directions represented in the map and the R values) should be interpreted as a proof of reliability. It is not believable that a random compilation of artificial, spurious solutions may give rise to such consistent stress pattern. So they should express an actual regional stress field.

The main feature of the stress field expressed by Fig. 3 is the dominant NW–SE trend of σ_3 trajectories. Nevertheless, some spatial variations may be noticed. In the northwestern sector σ_3 axes are mainly ESE, whereas in the central-southeastern sector they turn to SE or SSE. This is accompanied as well by a change in R. In the northwestern corner this parameter ranges between 0.10 and 0.48 (mean = 0.28), so it is significantly higher than the mean value in the rest of the studied region (0.10). As we explain in the following, this difference may be interpreted in the light of the tectonic evolution of the Ebro Basin. The last was controlled during the Neogene by two different geodynamic mechanisms, each one giving rise to its own primary stress field (Arlegui, 1996): (a) a N–S intraplate compressional field related to the convergence between Europe, Iberia and Africa; (b) a multidirectional extensional field linked to vertical isostatic movements in the boundary between the Pyrenean orogen and the foreland Ebro Basin. The N–S compression has been broadly documented from fault population and joint analysis in the Ebro Basin and surrounding areas (Simón, 1989; Hancock and Engelder, 1989; Hancock, 1991; Arlegui and Simón, 1993; Arlegui, 1996). The isostatically-controlled extension mainly affected the central and southeastern zone mapped in Fig. 3, where differential vertical movements concentrated into several NW–SE-striking basement faults. As they moved, they induced the development of normal faults of the same direction in the Tertiary cover, which may be observed as a highly penetrative tectolineament system in satellite images and aerial photographs (Arlegui *et al.*, 1994, 1997; Arlegui and Soriano, 1996). The intensity and horizontal trajectories of the extensional stress field were strongly controlled by this regional set of NW–SE faults. To the northwest their influence was nil, so that only the intraplate stress field is registered, showing N–S compression which evolves to coaxial E–W extension during the Miocene. In the central and southeastern Ebro Basin the resulting regional stress field may be interpreted as a superposition of both stress fields, although dominated by the local multidirectional extension. This shows NW–SE-trending σ_3 stress axes, parallel to macrostructural discontinuities, which may eventually undergo switching with the σ_2 axes (see stress directions obtained in stations Zar-2, Zar-7, Lon-7, Peñ-9, which trend near orthogonal to the regional tendency).

A QUANTITATIVE APPROACH TO THE INFLUENCE OF THE SAMPLE SIZE

In the previous sections we have seen how stability and reliability of palaeostress results increase as fault sample size increases, and how they can be estimated by using the subsampling/averaging technique. Now a further quantitative analysis of the previous results is necessary in order to answer two practical questions:

(a) What is the error and the probability associated with each palaeostress solution according to the size of the data sample?
(b) How can we decide the minimum number of data for defining an acceptable stress tensor? Is there any 'magic' number of faults which marks the boundary between 'bad' and 'good' solutions?

This new approach has been made by reprocessing and simplifying the data plotted on Fig. 7(a & b). We have reduced the symmetrical distributions showing positive and negative deviations of S_3 and R to absolute deviations. At the same time, we have substituted the scatter plots by two synthetic diagrams representing deviations of the two variables $(S_{3sam}-S_{3std})$ and $(R_{3sam}-R_{3std})$, respectively (Fig. 8a & b). Each diagram is made up by two percentile curves, 70 and 95%. As these curves show some irregularities in the actual data

distribution, the smoothed equivalents have been superposed by fitting exponential functions.

These curves can provide the answer for the questions stated before. First, the probable error in each case may be read directly. As an example, the smoothed curves of Fig. 8(a & b) indicate that 70% of stress tensors inferred from samples of 20 faults show a deviation of σ_3 lower than 8° and a deviation of R lower than 0.04 with respect to the optimum solutions; and 95% of them show a variation lower than 37° and 0.12, respectively. These variations may be considered as an estimate of the errors associated to an initial monophase sample of 20 faults, with a probability of 70 and 95%, respectively.

The question of the minimum sample size that should be used for defining the stress tensor depends upon the level of probability that we require. With a probability of 70%, it is evident that a sample of 15 faults (recommended by Etchecopar, 1984) may be enough to define the tensor with an error of only 13° in σ_3 and 0.06 in R (Fig. 8). With a probability of 95%, obviously these numbers increase considerably. Unfortunately, there is no 'magic' number of faults which clearly separates reliable from unreliable solutions, but the reported results may be a handy reference for facing the problem.

All these results have demonstrated to be useful for estimating palaeostress reliability in the Ebro Basin, where the fault samples used for their definition were collected. But, owing to the high number of data involved, they can also be a guide for evaluating palaeostress interpretations in other regions of the world affected by multidirectional extension stress fields. We should only remember that the level of ambiguity associated with the definition of stress directions in our case (with σ_3 being very similar to σ_2) is higher than that in cases of triaxial stress ellipsoids. So the errors expressed by curves of Fig. 8 are probably the maximum which may be expected. The size of fault samples in other more favourable stress regimes probably needs not be so large for attaining a certain level of stability.

CONCLUSIONS

The reliability of palaeostress interpretations from striated fault populations may be checked by applying a test based upon a *subsampling/averaging* procedure. The use of this test is advisable in areas undergoing a near multidirectional extensional stress field (σ_1 vertical, $\sigma_2 \approx \sigma_3$), such as the case of the central Ebro Basin. In these areas, it is sometimes difficult to define exactly the trends of the horizontal σ_2 and σ_3 axes, so that the reliability of results obtained by means of standard analysis may be questioned.

As a general rule, the stability of palaeostress solutions increases as the sample size grows. In multidirectional extension regime, the method of Etchecopar *et al.* (1981) provides very stable standard solutions from monophase fault samples made up by about 25–30 faults; for samples under 25 faults the results scatter, whereas the stability does not increase significantly for samples larger than 40 faults. The level of stability of the solutions is generally good. Most of individual stress tensors obtained after subsampling the initial data set differ less than 10° in σ_3 azimuth and 0.1 in stress ratio from the corresponding standard solutions.

According to the Central Limit Theorem (Till, 1974) and its application by Stuart (1984), stress tensors obtained by averaging solutions from groups of subsamples are more representative of the whole population than the result from a single sample. In any case, our final σ_3 directions and R values obtained by means of the subsampling/averaging technique only differ slightly with respect to the standard solutions computed from the initial samples (up to 18° for σ_3 azimuth and 0.15 for R). If those standard solutions

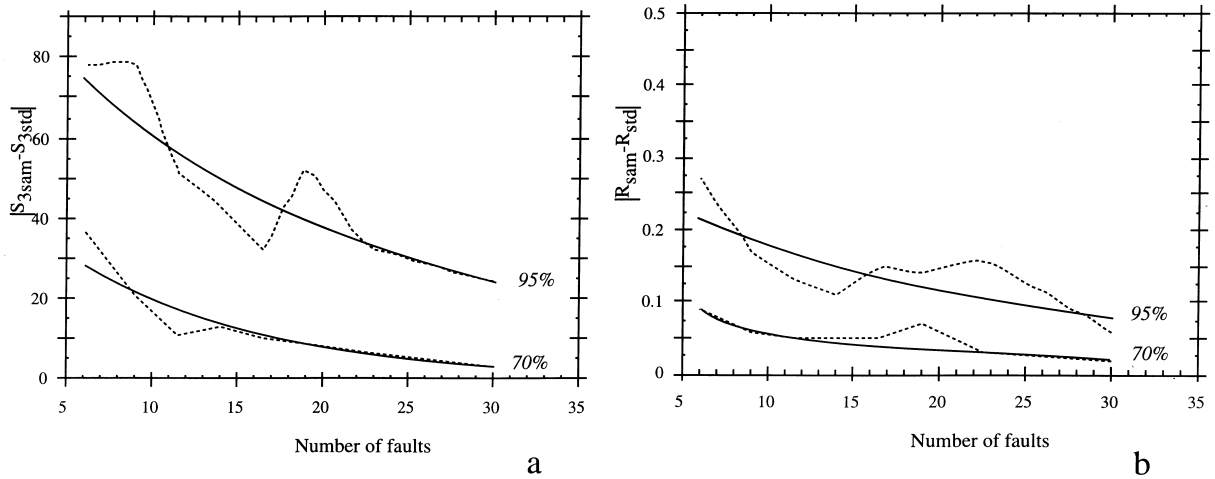

Fig. 8. Absolute deviations of stress tensors obtained from subsamples of different sizes, expressed for percentiles 70% and 95% (derived from diagrams of Fig. 7a & b). (a) S_3 deviations. (b) R deviations. Dotted: actual curves. Solid: smoothed curves drawn by fitting exponential functions.

would be only artefacts produced by random combinations of data one can expect that they would be quite a lot more unstable, so that any eventual spurious solution would vanish immediately after choosing any other fault subsample. On the other hand, the homogeneity of the final results all over the region (both the σ_3 directions and R values represented in the map of Fig. 3) should be interpreted as a proof of reliability. So they should represent an actual regional stress field.

The minimum number of faults needed for defining the stress tensor depends upon the error allowed and the level of confidence required. According to our results, the relation between these parameters within the multidirectional extension stress field of the Ebro Basin is shown in curves of Fig. 8. With a probability of 70%, a sample of 15 faults may be enough to obtain an acceptable result (error of only 13° in σ_3 and 0.06 in R). If 95% confidence is required, a sample of 30 faults is needed for accomplishing errors under 25° and 0.08, respectively. As a practical rule, data collection should be as intensive as possible. Monophase fault samples should necessarily include more than 15 faults, although measuring 25–30 will be better. On the other hand, no significant improvement will be obtained for samples exceeding 40 faults.

These results should be considered as a general reference for evaluating stability and reliability of palaeostress reconstructions in near uniaxial stress regimes. They probably represent a less favourable case than triaxial stress states, in which errors in stress axis orientations are expected to be smaller. The subsampling/averaging technique needs not to be considered as necessary in every palaeostress analysis. Stability and reliability of stress tensors inferred from samples larger than 25–30 faults are guaranteed for most uniaxial and triaxial stress states. If a bad result arises from a sample of such size, it will probably be due to some bias, and it will not be improved by any procedure. Only for samples under 20–25 faults in uniaxial stress regimes (especially in the quite usual case of multidirectional extension) may the subsampling/averaging technique be a useful tool. It allows testing and, in some special cases (those where subsample mean tensors provide stable results which systematically differ from the initial standard tensor), improving of stress solutions.

Acknowledgements—The authors are very grateful to Richard J. Lisle for his constructive suggestions on the first version of the manuscript. The review and helpful comments by Martin G. Miller and Don Wise are also acknowledged. The research has been supported by projects PB93-1218 of the C.I.C.Y.T. (Spanish Government) and JOU2-CT94-0208 of the European Commission.

REFERENCES

Angelier, J. and Mechler, P. (1977) Sur une méthode graphique de recherche des contraintes principales également utilisable en tectonique et en séismologie: la méthode des dièdres droits. *Bulletin Societé Géologique de la France* **19,** 1309–1318.

Arlegui, L. E. (1996) Diaclasas, fallas y campos de esfuerzos en el sector central de la Cuenca del Ebro. Unpublished Ph.D. thesis, Universidad de Zaragoza.

Arlegui, L. E. and Simón, J. L. (1993) El sistema de diaclasas N–S en el sector central de la Cuenca del Ebro. Relación con el campo de esfuerzos neógeno. *Revista de la Sociedad Geológica de España* **6,** 115–123.

Arlegui, L. E., Soriano, A. and Simón, J. L. (1994) Un sistema regional de fracturas NW–SE en el Centro de la Cuenca del Ebro. *2° Congreso Grupo Español del Terclario*. 39–43.

Arlegui, L. E. and Soriano, A. (1996) Lineamientos y su influencia en los modelados del centro de la Cuenca del Ebro, IV Reunión Nacional de Geomorfología, O Castro-Sada. La Coruña.

Arlegui, L. E., Simón, J. L. and Soriano, M. A. (1997) Estructuración neógena del sector central de la Cuenca del Ebro. In *Avances en el conocimiento del Terciario Ibérico*, eds J. P. Calvo and J. Morales, pp. 33–37. UCM-CSIC.

Armijo, R. (1977) La zone de failles de Lorca–Totana (Cordillères Bétiques, Espagne). Etude tectonique et néotectonique. Unpublished Ph.D. thesis, Université Paris VII.

Bott, M. H. P. (1959) The mechanics of oblique slip faulting. *Geological Magazine* **96,** 109–117.

Caputo, R. (1995) Evolution of orthogonal sets of coeval extension joints. *Terra Nova* **7,** 479–490.

Casas, A. M., Gil, I. and Simón, J. L. (1990) Los métodos de análisis de paleoesfuerzos a partir de poblaciones de fallas: sistemática y técnicas de aplicación. *Estudios geológicos* **46,** 385–398.

Casas, A. M., Serón, F. J. and Simón, J. L. (1992) Stress deflection in a tectonic compressional field: a model for the Northwestern Iberian Chain, Spain. *Journal of Geophysical Research* **97,** 7183–7192.

Casas, A. M. and Maestro, A. (1996) Deflection of a compressional stress field by large scale basement faults. A case study from the Tertiary Almazán Basin (Spain). *Tectonophysics* **255,** 135–156.

Dunne, W. M. and North, C. P. (1990) Orthogonal fracture systems at the limits of thrusting: an example from southwestern Wales. *Journal of Structural Geology* **12,** 207–215.

Etchecopar, A. (1984) Etude des états de contraintes en tectonique cassante et simulations de déformations plastiques (approche matématique). Unpublished Ph.D. thesis. USTL Montpellier.

Etchecopar, A., Vasseur, G. and Daignières, M. (1981) An inverse problem in microtectonics for the determination of stress tensors from fault striation analysis. *Journal of Structural Geology* **3,** 51–65.

Fry, N. (1992) Stress ratio determinations from striated faults: a spherical plot for cases of near-vertical principal stress. *Journal of Structural Geology* **14,** 1121–1131.

Galindo, J. and González, F. (1988) Faulting phase differentiation by means of computer search on a grid pattern. *Annales Tectonicae* **2,** 90–97.

Gephart, J. W. (1990) FMSI: A Fortran program for inverting fault/slickenside and earthquake focal mechanism data to obtain the regional stress tensor. *Computers and Geosciences* **16,** 953–989.

Hancock, P. L. (1985) Brittle microtectonics: principles and practice. *Journal of Structural Geology* **7,** 437–457.

Hancock, P. L. (1991) Determining contemporary stress directions from neotectonic joint systems. *Philosophical Transactions of the Royal Society of London A* **337,** 29–40.

Hancock, P. L., Kadhi, A., Barka, A. A. and Bevan, T. G. (1987) Aspects of analysing brittle fractures. *Annales Tectonicae* **1,** 5–19.

Hancock, P. L. and Engelder, T. (1989) Neotectonic joints. *Geological Society of America Bulletin* **101,** 1197–1208.

Park, R. G. (1983) *Foundations of Structural Geology*. Blackie, Glasgow.

Pegoraro, O. (1972) Application de la microtectonique à un étude de néotectonique. Le golfe Maliaque (Grèce centrale). Unpublished Ph.D. thesis, USTL Montpellier.

Petit, J-P. (1987) Criteria for the sense of movement on fault surfaces in brittle rocks. *Journal of Structural Geology* **9,** 597–608.

Quirantes, J. (1978) Estudio sedimentológico y estratigráfico del Terciario Continental de los Monegros. *Publicación 681 Institución Fernando el Católico, Zaragoza*, 207.

Reches, Z. (1987) Determination of the tectonic stress tensor from slip along faults that obey the Coulomb yield criterion. *Tectonics* **6,** 849–861.

Reches, Z., Baer, G. and Hatzor, Y. (1992) Constraints on the strength of the Upper Crust from stress inversion of fault slip data. *Journal of Geophysical Research* **97,** 12,481–12,493.

Riba, O., Reguant, S. and Villena, J. (1983) Ensayo de síntesis estratigráfica y evolutiva de la cuenca terciaria del Ebro. Libro Jubilar J.M. Ríos, Geología de España, IGME.

Simón-Gómez, J. L. (1986) Analysis of a gradual change in stress regime (example from the eastern Iberian Chain, Spain). *Tectonophysics* **124,** 37–53.

Simón-Gómez, J. L. (1989) Late Cenozoic stress field and fracturing in the Iberian Chain and Ebro Basin (Spain). *Journal of Structural Geology* **11,** 285–294.

Simón, J. L., Serón, F. J. and Casas, A. M. (1988) Stress deflection and fracture development in a multidirectional extension regime. Mathematical and experimental approach with field examples. *Annales Tectonicae* **2,** 21–32.

Stuart, A. (1984) *The Ideas of Sampling*. C. Griffin, High Wycombe.

Till, R. (1974) *Statistical Methods for the Earth Sciences*. John Wiley & Sons, New York.

Turner, J. P. and Hancock, P. L. (1989) Relationships between thrusting and joint systems in the Jaca thrust-top basin. Spanish Pyrenees. *Journal of Structural Geology* **12,** 217–226.